Particle Image Velocimetry Measurements to Evaluate the Effectiveness of Deck-Edge Columnar Vortex Generators on Aircraft Carriers

Drew Landman
Department of Aerospace Engineering, Old Dominion University, Norfolk, VA 23529

dlandman@odu.edu

John E. Lamar
NASA Langley Research Center, Hampton, VA 23681-2199

John.E.Lamar@nasa.gov

Russell Swift
Department of Aerospace Engineering, Old Dominion University, Norfolk, VA 23529

ABSTRACT

Candidate passive flow control devices were chosen from a NASA flow visualization study to investigate their effectiveness at improving flow quality over a flat-top carrier model. Flow over the deck was analyzed using a particle image velocimeter and a 1/120th scaled carrier model in a low-speed wind tunnel. Baseline (no devices) flow quality was compared to flow quality from combinations of bow and deck-edge devices at both zero and 20 degrees yaw. Devices included plain flaps and spiral cross-section columnar vortex generators attached in various combinations to the front and sides of the deck. Centerline and cross plane measurements were made with velocity and average turbulence measurements reported. Results show that the bow/deck-edge flap and bow/deck-edge columnar vortex generator pairs reduce flight deck turbulence both at zero yaw and at 20 degrees yaw by a factor of approximately 20. Of the devices tested, the most effective bow-only device appears to be the plain flap.

1.0 INTRODUCTION

Naval flight operations from aircraft and helicopter carriers present many challenges to pilots. The bluff shapes of aircraft carrier flight deck edges can create extremely unsteady turbulent flows over the flight deck with areas of separation and high vorticity. This flow creates unpredictable and often dangerous situations for aircraft and rotorcraft during landing and takeoff [1-3]. On flat-top carriers, the air flow over the flight deck is primarily influenced by the flight deck edges and corners with some contributions from the bridge island tower and on/over deck aircraft. On frigates/destroyers, the flight deck is often directly behind the bridge and thus the flow shed off the tower dominates the region. Recently a group of researchers from various NATO countries have devoted resources, as a part of a task group sponsored by the Research and Technology Organization (scientific arm of NATO), to the assessment of novel flow control devices and methods specifically to improve flow over the deck. As a part of NASA's contribution to the NATO program, Langley conducted two low-speed, preliminary qualitative (visual data) wind-tunnel tests, the results of which are unpublished. The first test was in its Subsonic Basic Research Tunnel (SBRT), used smoke flow over both isolated devices and with a partial carrier model, and was considered to be an initial effort. The second test

was performed in the 14 ft by 22 ft tunnel using a laser-light sheet and smoke for many different devices mounted onto a 1/120th scaled carrier model. Results from the second test showed that qualitative changes occurred in the flow-field due to these devices and justified further study using a quantitative experimental measurement technique. A Particle Image Velocimetry (PIV) study was conducted at ODU by the third author on a subset of novel flow control devices from the second test and the resulting data are the primary subject of this paper.

The basic carrier flow problem is illustrated well in figure 1 by a computational fluid dynamic (CFD) image from a companion study to the experimental work presented below. The typical pattern of leading edge separation followed by an area of recirculation and high vorticity is illustrated. In addition to the leading edge separation, the side deck edges may generate strong vortical flows that can extend onto the flight operations area and are characteristically unsteady. At yaw, the side deck edges play a larger role in the turbulent over-the-deck flows.

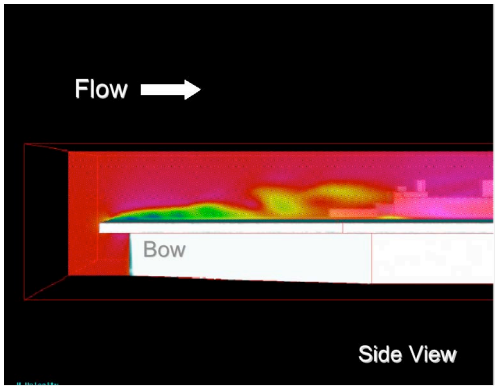

Figure 1 Leading Edge Separation at Flat-Top Carrier Bow

2.0 COLUMNAR VORTEX GENERATORS (CVG)

A columnar vortex generator is one of the novel flow control devices tested and, as originally envisioned for a frigate/destroyer, it consists of a spiral shaped open cylinder, closed at one end, with tangential flow ingress and axial flow egress. In theory, a shear layer may enter the device tangentially and exit the device as a vortex [4]. With little guidance from the literature as to dimensions and design, a test was devised to evaluate the efficacy of the CVG concept. A range of CVG's were designed to capture key geometric parameters, fabricated at the Langley stereo-lithography laboratory, and subsequently tested in the 22 in by 32 in SBRT. Each CVG was made ten inches long with inner and outer radii varying from one half inch to two inches. The goal of the testing was to ascertain if they could capture flow through a tangential gap and then generate, due to the axial flow interacting with the internal spiral construction of the CVG, a vortex at the open end that would persist downstream. Two CVG concepts and a photograph from a smoke flow visualization test are shown in figure 2.

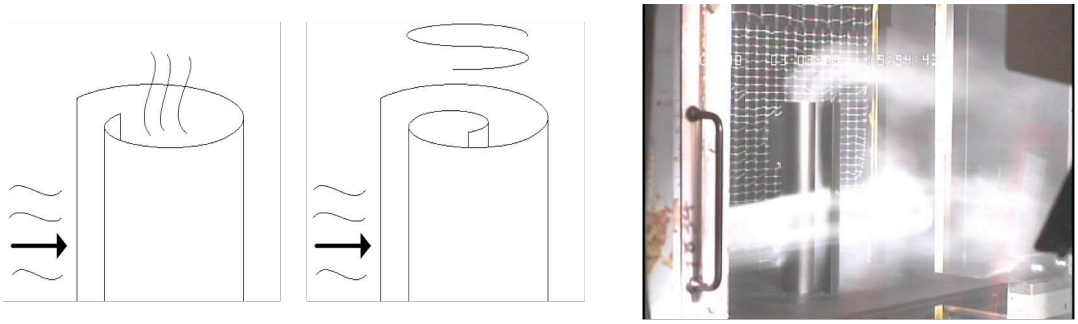

Figure 2 Columnar Vortex Generators and Smoke Flow Visualization in SBRT

Application of one or more CVGs to a carrier model followed when it was realized that they could possibility be used to organize and direct the deck-edge flow if they were mounted horizontally and were open ended. CVGs attached in this manner to a 1/120th scaled carrier model are shown later.

3.0 PARTICLE IMAGE VELOCIMETRY

Particle Image Velocimetry is a laser based flow diagnostic technique that has achieved recent popularity among fluid dynamics researchers. The benefits include a non-intrusive direct measurement of a velocity field in a fluid over a wide speed range from 1 m/s up to supersonic velocities. With successive measurements of velocity, vector maps, statistics, spatial correlations, and other relevant data are recovered. Both two and three velocity component versions of PIV systems are commercially available. What follows is a brief description of the two component system used in the present study [5].

The fundamental hardware inherent to a PIV system includes the planar light source, scientific grade CCD camera, synchronizing electronics, flow seeder, and a computer with a "frame grabber" board. Typically a pair of lasers with cylindrical and spherical lenses are used to create a planar light sheet that can be pulsed twice in rapid succession. The laser light sheet is positioned over the region of interest and the camera is positioned normal to the sheet. A mineral oil flow seeder is used to inject micron sized particles into the flow field. The lasers are commanded to fire two bursts in rapid succession while the seed particle images are recorded in two frames by synchronizing the CCD camera. Velocity vectors are derived from sub-sections of the target area of the particle-seeded flow by measuring the movement of particles between the two light pulses. Once a sequence of two light pulses is recorded, the images are divided into small subsections called interrogation areas. The interrogation areas from each image frame, are cross-correlated with each other, pixel by pixel.

Manufacturer:	TSI
Camera:	PIVCAM 13-8, 1.3 Megapixel, 8 hz max, 12 bit resolution
Camera interface:	TSI Laserpulse synchronizer, commercial frame grabbers
Laser:	New Wave Y50-15 Dual YAG, 50 mJ/pulse, 15 pulses/sec max.
Seeding:	Mineral oil, ROSCOE fogger
Software:	TSI Insight
Host Computer:	Dell personal computer, dual processor, Windows OS
Max PIV rate (2D):	3.75 hz

Table 1 ODU PIV System Specifications

The correlation produces a signal peak, identifying the common particle displacement, Δx. A velocity vector map over the whole target area is obtained by repeating the cross-correlation for each interrogation area over the two image frames captured by the CCD camera. By knowing the time difference between pulses (Δt) and particle displacements (Δx), a direct calculation of the velocity may be computed as $\Delta x/\Delta t$. Repeating this process for each interrogation area yields the instantaneous velocity field. For a comprehensive discussion of the technique the reader is directed to reference 5.

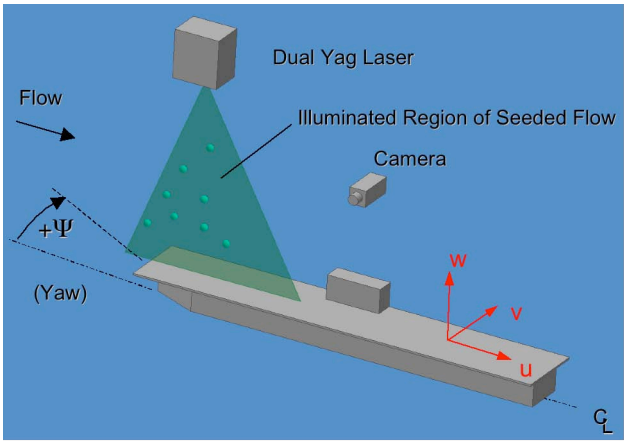

Figure 3 PIV Component Orientation for Centerline Measurement

The specifications for the Old Dominion University (ODU) Department of Aerospace

Engineering PIV system are provided in table 1. The system is capable of resolving velocity vector fields at the rate of 3.75 measurements per second (hz). The physical size of the imaged light sheet is approximately 8.5 x 12 inches. The orientation of the PIV components for a centerline measurement on a carrier model is shown in figure 3. Using the notation of the figure, in-plane velocity components u and w are measured using this configuration.

4.0 EXPERIMENT OVERVIEW

The use of CVG's to control carrier deck edge separation was proposed. A wind tunnel experiment, using a 1/120th scaled LHD carrier was devised in order to evaluate device performance. Devices were placed along the bow leading edge as shown in figure 4, both alone and with devices on the (longitudinally oriented) side edges as shown in figure 5. It should be noted that the side edge devices only extended from the bow to a location 16.5 inches aft, this was thought to be sufficient to capture the primary effect. The PIV system was used to measure instantaneous velocity fields and to gather statistics to assess turbulence and vorticity levels. Two dimensional velocity field measurements were made in a plane on the carrier deck centreline, in a plane

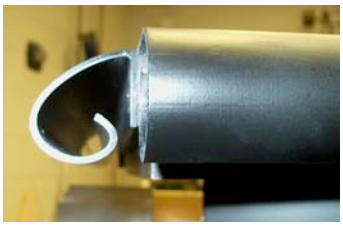

Figure 4 Carrier Model with Bow CVG

Figure 5 Carrier Model with Port Deck Edge CVG

Run	Camera and Laser Setup	Model Configuration
1	Side Camera | Longitudinal Centerline Laser Plane	Baseline, 0° Yaw
2		Bow CVG, 0° Yaw
3		Bow Flap, 0° Yaw
4	Side Camera | Longitudinal Starboard Edge Laser Plane	Bow Flap, 0° Yaw
5		Bow Flap, 0° Yaw
6		Bow CVG, 0° Yaw
7		Baseline, 0° Yaw
8	Side Camera | Longitudinal Centerline Laser Plane	Baseline, 20° Yaw
9		Bow Flap, 20° Yaw
10		Bow CVG, 20° Yaw
11		Bow and Side CVG's, 20° Yaw
12		Side CVG, 20° Yaw
13		Side Flap, 20° Yaw
14		Bow and Side Flaps, 20° Yaw
15	Rear Camera | Lateral 10" from Bow Laser Plane	Bow and Side Flaps, 20° Yaw
16		Baseline, 20° Yaw
17		Bow Flap, 20° Yaw
18		Side CVG, 20° Yaw
19		Bow and Side CVG, 20° Yaw
20		Bow CVG, 20° Yaw
21		Bow CVG, 0° Yaw
22		Baseline, 0° Yaw
23		Bow Flap, 0° Yaw

Table 2 Experiment Test Matrix

parallel to the centreline but at the starboard deck edge, and in a lateral cross plane in the region of strong recirculation, 10 inches from the bow. A yaw angle was chosen to assess the sensitivity to cross winds, both a

zero and 20 degree yaw were evaluated. The entire test matrix is provided in table 2.

For the centerline measurements (both at zero yaw and at 20 degrees yaw), the camera viewed the laser sheet through a window in the test section of the wind tunnel. The laser sheet was projected from a window above. For cross plane measurements the camera was moved to a downstream location in the flow and the laser assembly was rotated 90 degrees. The orientation of the model and the PIV system for both longitudinal and lateral velocity field measurements is shown in the schematics of figure 6 and 7. PIV measurements at yaw were conducted by rotating the model, camera and laser 20 degrees to maintain the relative optical distances.

5.0 EXPERIMENTAL DETAILS

5.1 Facility Description

The Old Dominion University Low Speed Wind Tunnel (LSWT) is a closed return, fan driven, atmospheric pressure tunnel driven by a 125 horsepower electric motor. As shown in figure 8, the tunnel has a unique dual test section design. The high speed section measures 3 ft by 4 ft in cross section and is 8 feet long with maximum speeds of approximately 175 ft/s. The low speed test section located upstream measures 7 ft by 8 ft in cross section, is 7 feet long, and has a maximum speed of approximately 37 ft/s. The average freestream turbulence intensity measured in the high speed test section is 0.2 %. Wind tunnel velocity is computed from differential pressure measurements across the tunnel contraction cone, temperature measurement in the high speed test section from a thermocouple, and atmospheric pressure from a mercury barometer. All experimental runs were conducted in the low-speed test section at a nominal velocity of 33 ft/s.

A raised ground board with semicircular leading edge cross section was inserted in the low-speed test section so as to divide the flow in half. The model was then nominally positioned on the centerline of the ground plane. The model in the test section is shown in figure 9.

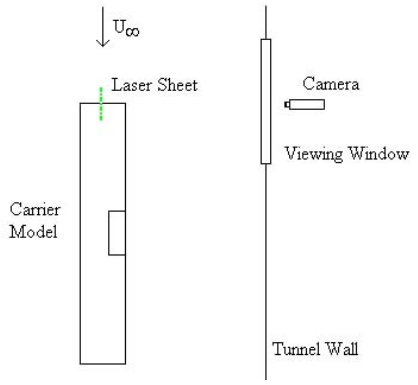

Figure 6 PIV System and Model Location for Longitudinal Velocity Measurements

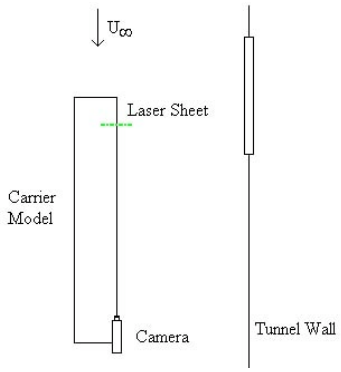

Figure 7 PIV System and Model Location for Lateral Velocity Measurements

5.2 LHD Carrier Model

A 1/120th scaled LHD flat top carrier model was borrowed from NASA Ames Research Center. The model has overall dimensions of 80 inches long, 12 inches wide, and 14 inches tall and represents a

simplified light helicopter carrier. The representation of the island measures 17 inches long by 4.375 inches wide by 5 inches tall (above the deck). A new flight deck was fitted with integral mounting rails to accommodate simple flow control device mounting. No fasteners or other protuberances were required. The model, shown in figure 10, was fixed to a raised ground board for the two yaw angles tested.

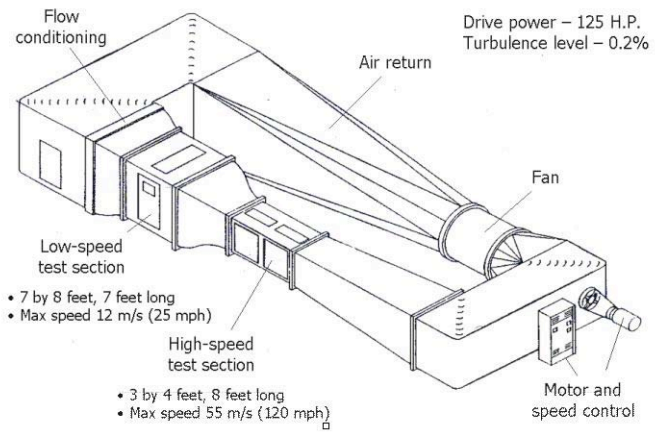

Figure 8 The Old Dominion University Low-Speed Wind Tunnel

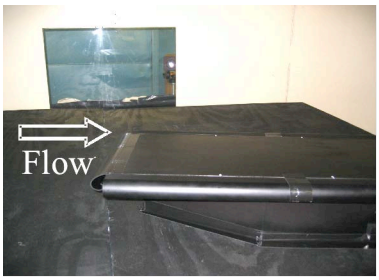

Figure 9 LHD in ODU LSWT

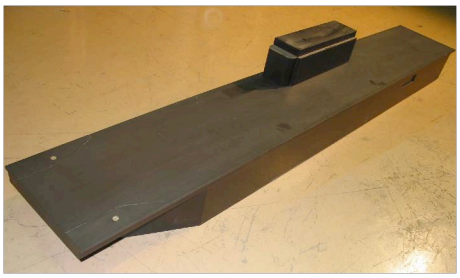

Figure 10 Simplified Baseline LHD Carrier Model

5.3 Deck-edge Devices Tested

Four devices were chosen for this study, two for the bow, and two for the longitudinal deck side edges. The bow CVG and flap are detailed in figure 11 and the deck-edge CVG and flap are shown in figure 12. All devices were constructed of resin using the stereo lithography process at NASA LaRC.

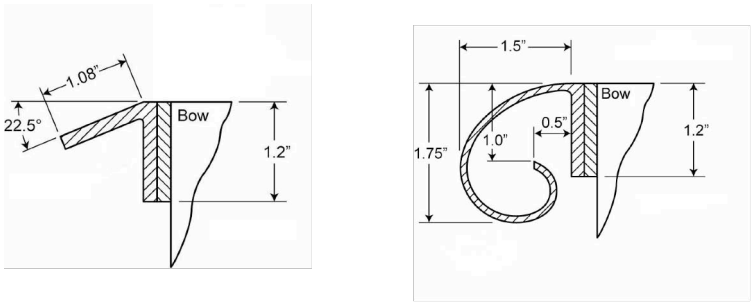

Figure 11 Bow Devices Tested

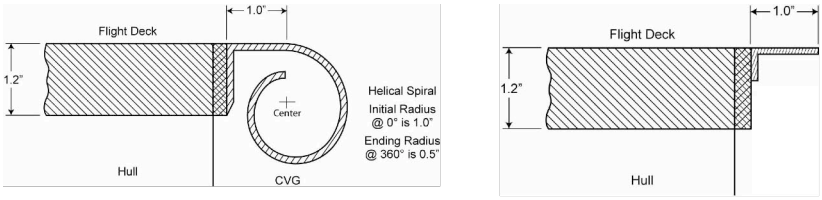

Figure 12 Deck Edge Devices Tested

6.0 RESULTS AND DISCUSSION

The nature of this experiment was to evaluate the effectiveness of prototype devices in a more quantitative manner than was done previously in the 14 ft by 22 ft tunnel test. The ODU wind tunnel simulation was not perfect due to several key factors [6]. These include: (1) The blockage is rather high as the model is very large for the test section; (2) the Reynolds number is low in comparison to the full scale vehicle; (3) the model fidelity is rather crude; and (4) the atmospheric boundary layer was not simulated correctly. Despite the negation of these important details, the experiment did capture the basic flow physics [3] and should serve as a foundation for further research and design work.

During this test, 100 image pairs were taken per run at a rate of approximately 3.75 image pairs per second (hz). Statistical information was calculated over those 100 images. Non-lighted areas in the field of view of the camera were masked to blend in with the black background for clarity. It should be noted that spurious

results from poor lighting conditions were removed from the average turbulence and vorticity plots.

All PIV results are presented following the Reference section of the text. A sample of the raw computed (mean) velocity vectors from runs 1-3 is shown in figures 13-15. These centerline velocity vector images immediately showed that both bow devices reduced leading edge separation and hence the downstream turbulence dramatically compared to the baseline case. The white dashed lines were added to show the approximate geometry of the test model. It should be noted that the starboard deck-edge laser plane location of runs 4-7 provided little useful information due to the laser striking the visible side of the model and thus creating large regions that the PIV software couldn't evaluate properly – these runs were omitted from the results. Runs 8-23 provided valuable turbulence results. The rear view raw vector images of runs 15-23 showing low-magnitude cross flows and the effect of the side devices were not as revealing as their side view counterparts. The resulting raw vector images were more difficult to interpret directly and were omitted for brevity in favor of showing the turbulence results.

Node **average turbulence** is calculated by dividing the standard deviation of the velocity values from the 100 sample image pairs by the average velocity at each node. Results are presented as a percentage. Vorticity is calculated at each node using the following relation and is presented as a percentage:

$$vorticity = \frac{\left(\frac{\partial v}{\partial x}\right) - \left(\frac{\partial u}{\partial y}\right)}{2.0}$$

Comparing figures 16, 17, and 18 (all at zero yaw) it is clear that both the bow devices significantly reduce the turbulence from well over 100% to well below 5% by eliminating the circulation bubble. The extent of the bubble may be exaggerated when these results are compared to full scale carriers due to the low Reynolds number [3]. The bow edge CVG appears to be equally effective at reducing turbulence when compared to the 22.5 degree bow flap. Figures 19-21 show that the plain bow flap (only) and bow CVG (only) reduce turbulence at the yawed condition, whereas the plain flap may be more effective. Figures 22 and 23 show that the bow CVG / side CVG and bow flap / side flap combinations reduce turbulence on the deck centerline at yaw to the magnitude seen in the zero yaw cases with only the bow devices in place. A side flap and side CVG (only) case was run for completeness and showed (as expected) little effectiveness at yawed conditions. Figure 24 shows the deck centerline flow (side view) under the presence of the side CVG only at yaw.

Turning to the rear views, figures 25-27 show the rear view of the deck with the starboard edge centered in the images. The baseline case (figure 25) shows the large deck area affected by turbulence. Figures 26 and 27 reveal the powerful attenuation of turbulence provided by the bow devices. Figures 28 and 29 - rear view – show the benefit of employing bow and deck edge devices together in that the over-the-deck turbulence level is attenuated by a factor of approximately 20. In figure 30 the rear view of the side CVG only is provided for completeness and shows no benefit when acting alone.

Vorticity calculations revealed similar information when compared to the turbulence calculations. In figures 31 and 32, the effectiveness of the bow CVG may be seen. Comparing these figures to 16 and 17 shows the same effected area over the deck. From a quantitative standpoint, the vorticity calculations confirm the turbulence level data already presented.

7.0 CONCLUSIONS

PIV measurements provided an excellent tool for evaluating the effectiveness of carrier deck-edge devices at reducing flight-deck turbulence. The resulting turbulence levels provided a clear picture of flow quality improvement in the plane of interest with no aerodynamic interference for the small number of devices tested. Moreover, the method and results were promising and these will prove useful in the future for investigating additional devices. Sample vorticity measurements corroborated well with the average turbulence measurements for the bow CVG.

The use of deck-edge devices in combination with bow-edge devices produced the best results in terms of lowering over-the-deck turbulence levels for the tested yaw angle of 20 degrees. The reduction in the turbulence level is on the order of a factor of 20. Both the CVG and the plain flaps proved effective when used on the bow and side edges. The bow-flap alone represents a good compromise in providing turbulence reduction with a very simple geometry. If these devices were to be considered for use on fleet aircraft carriers, it would most likely be more practical to add an angled bow flap than to create a curved surface around the entire deck edge.

It should be noted that these tests were conducted at Reynolds numbers much lower than the full-scale conditions. Referenced CFD, wind-tunnel and full scale tests have shown the same fundamental flow structures in the small scale model testing conducted here, but with the baseline full-scale patterns showing reattachment to occur more forward at zero yaw.

Acknowledgements

The authors gratefully acknowledge the design suggestions made by Dr. Raj K. Nangia of Nangia Aero Research Associates regarding the cross-sectional shapes of the novel flow devices to be tested and the help provided by Dr. Colin P. Britcher of ODU with the PIV system.

8.0 REFERENCES

[1] Lumsden, R. Bruce, “Ship Air-Wake Measurement, Prediction, Modeling and Mitigation,” DSTL/TR06951, April, 2003

[2] Polsky, S., “A Computational Study of Unsteady Ship Wake,” *AVT Symposium*, Loen, Norway, May 2001

[3] Czerwiec, Ryan; and Polsky, Susan A.: LHA Airwake Wind Tunnel and CFD Comparison with and without Bow Flap. AIAA paper AIAA-2004-4832, presented at the AIAA 22nd Applied Aerodynamics Conference and Exhibit in Providence RI, August 16-19, 2004

[4] Lugt, Hans J.: Vortex Flow in Nature and Technology. John Wiley & Sons 1983, p. 143.

[5] Raffel, M., Willert, C., and Kompenhans, J., *Particle Image Velocimetry*, Springer-Verlag, New York, 1998.

[6] Barlow, J.B., Rae, W.H., and Pope, A., Low Speed Wind Tunnel Testing, 3rd ed., John Wiley and Sons, 1999

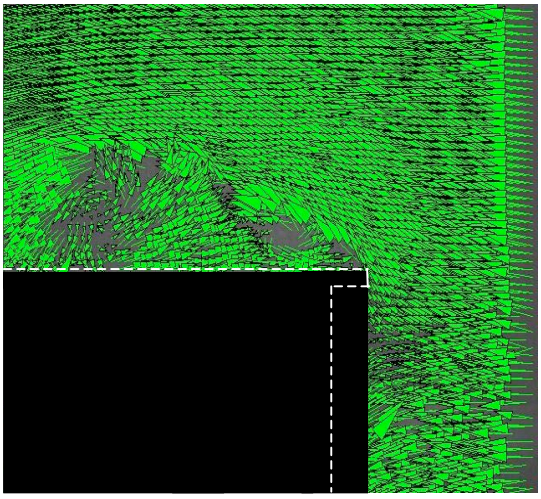

Figure 13

Velocity Vectors

Centerline

Yaw = 0 deg

Baseline Bow

Side View

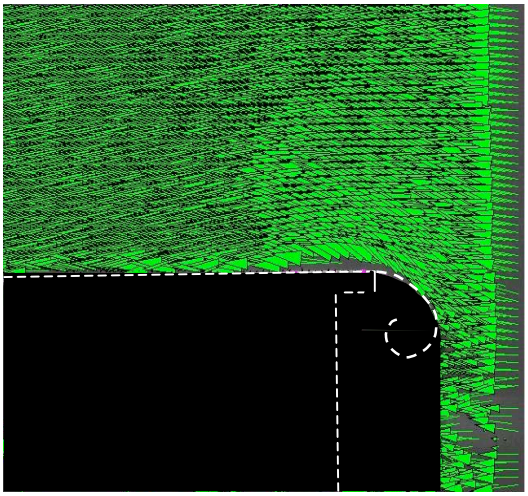

Figure 14

Velocity Vectors

Centerline

Yaw = 0 deg

Bow CVG

Side View

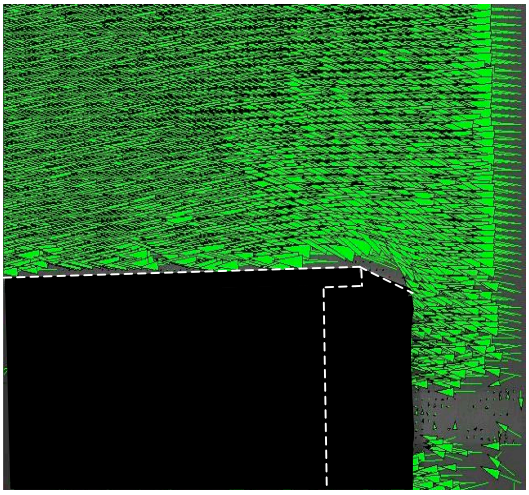

Figure 15

Velocity Vectors

Centerline

Yaw = 0 deg

Bow Flap

Side View

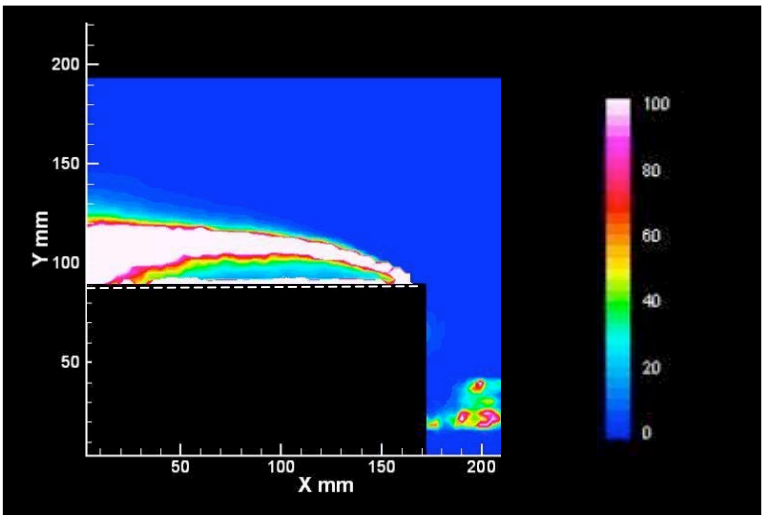

Figure 16

% Avg. Turbulence

Centerline

Yaw = 0 deg

Baseline Bow

Side View

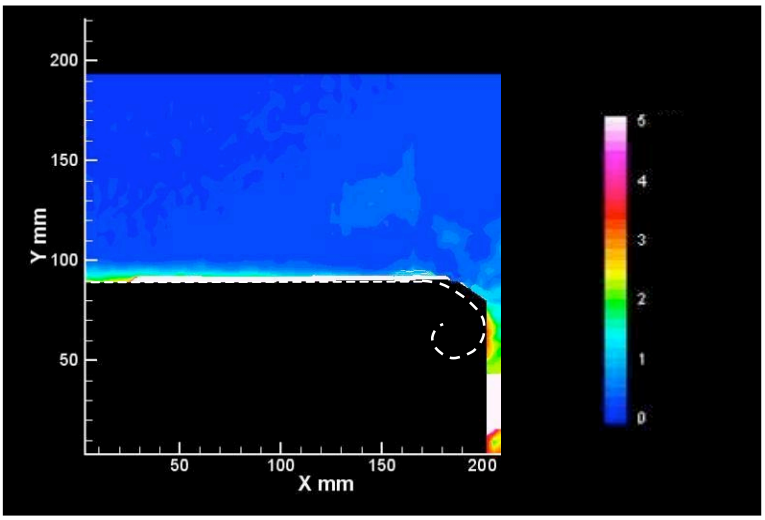

Figure 17

% Avg. Turbulence

Centerline

Yaw = 0 deg

Bow CVG

Side View

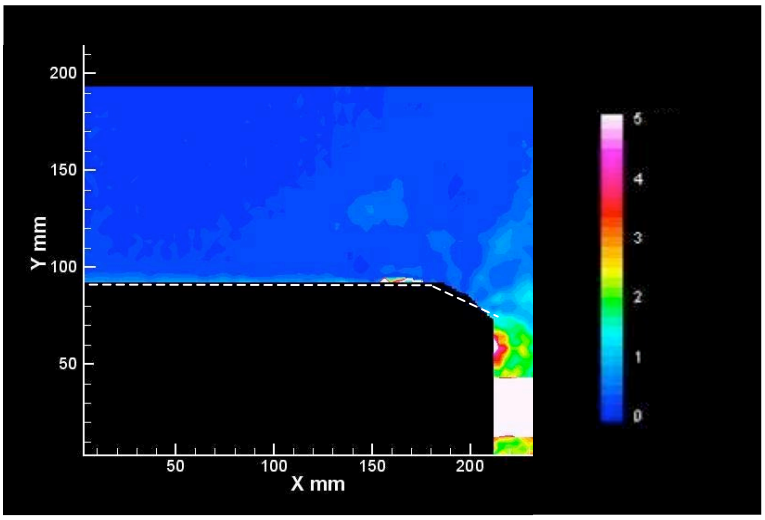

Figure 18

% Avg. Turbulence

Centerline

Yaw = 0 deg

Bow Flap

Side View

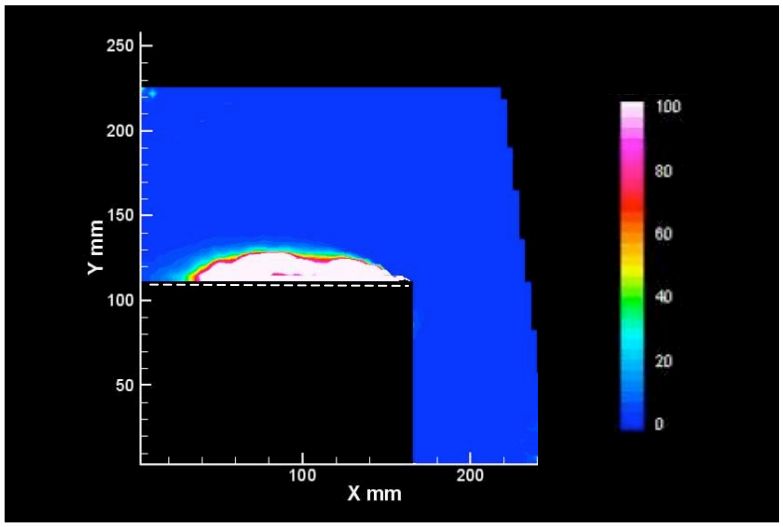

Figure 19

% Avg. Turbulence

Centerline

Yaw = 20 deg

Baseline Bow

Side View

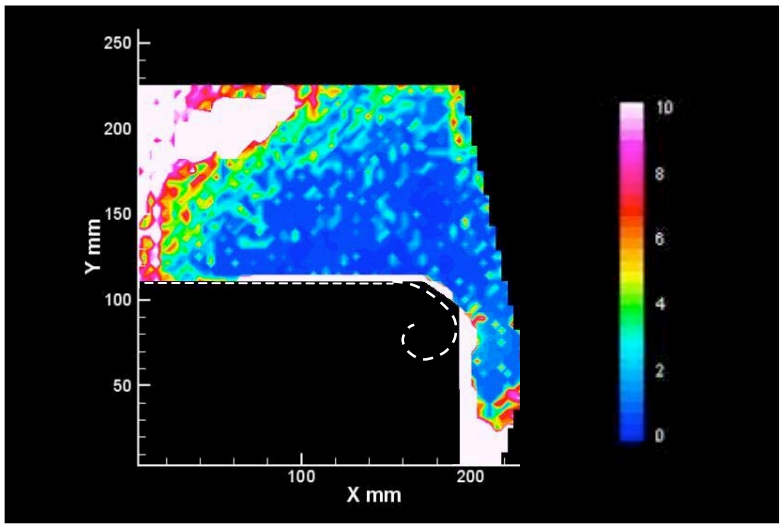

Figure 20

% Avg. Turbulence

Centerline

Yaw = 20 deg

Bow CVG

Side View

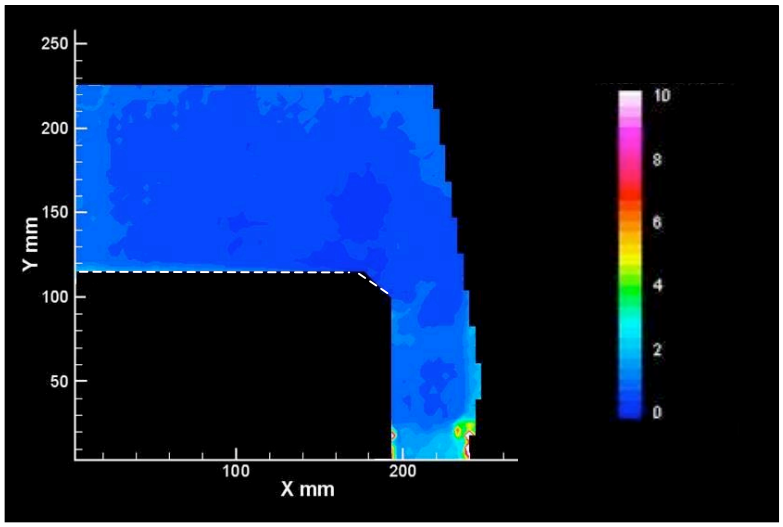

Figure 21

% Avg. Turbulence

Centerline

Yaw = 20 deg

Bow Flap

Side View

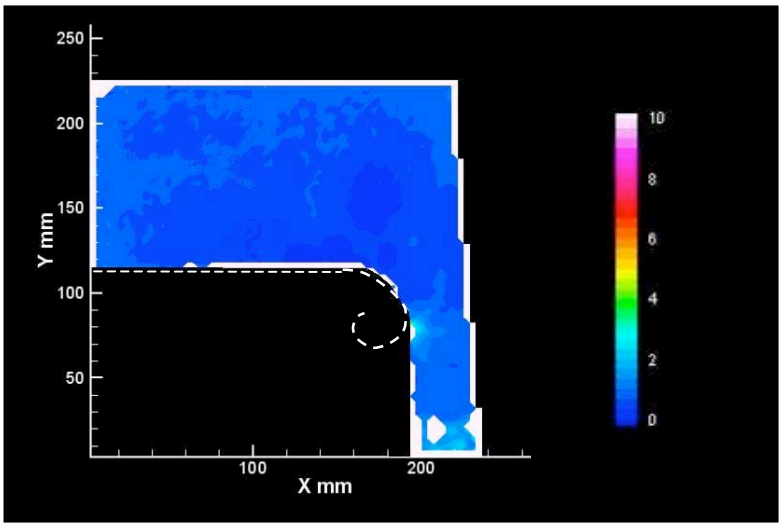

Figure 22

% Avg. Turbulence

Centerline

Yaw = 20 deg

Bow and Side CVG

Side View

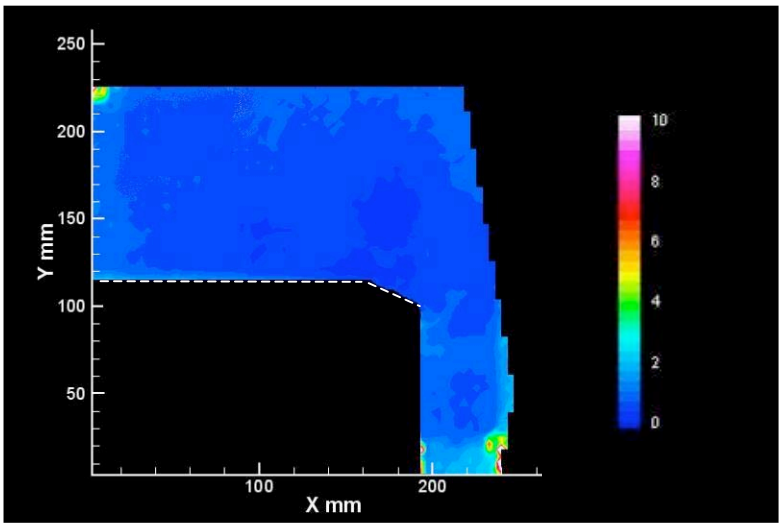

Figure 23

% Avg. Turbulence

Centerline

Yaw = 20 deg

Bow and Side Flap

Side View

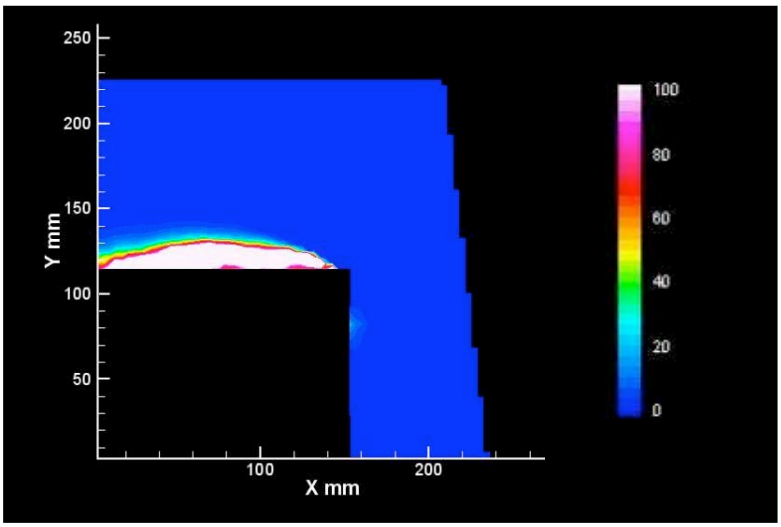

Figure 24

% Avg. Turbulence

Centerline

Yaw = 20 deg

Side CVG Only

Side View

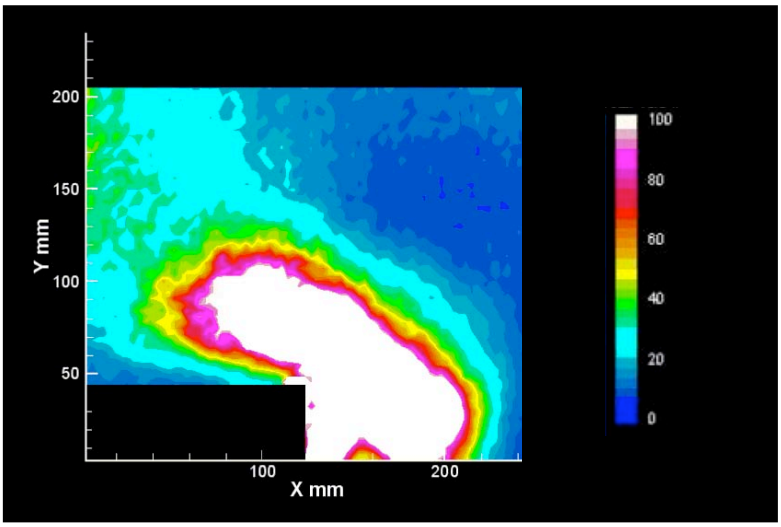

Figure 25

% Avg. Turbulence

Yaw = 20 deg

Baseline Bow

Rear View

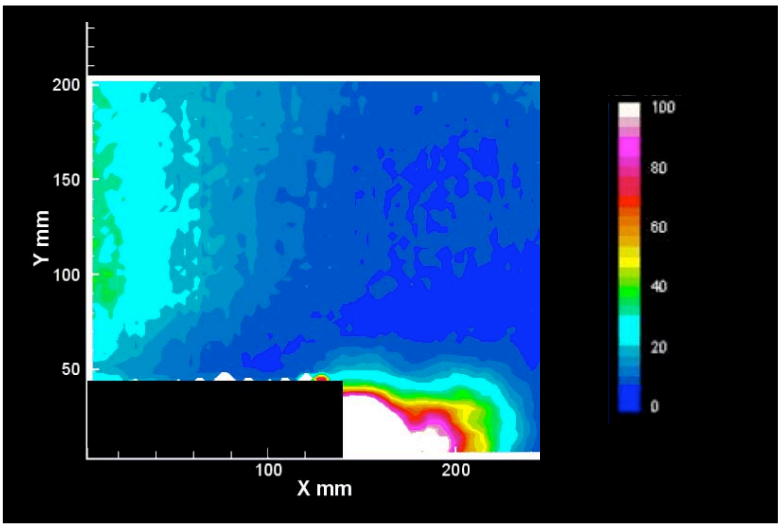

Figure 26

% Avg. Turbulence

Yaw = 20 deg

Bow CVG

Rear View

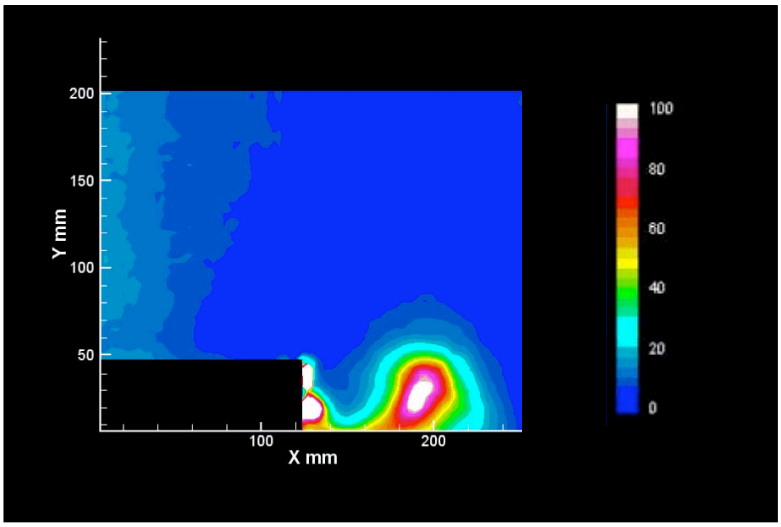

Figure 27

% Avg. Turbulence

Yaw = 20 deg

Bow Flap

Rear View

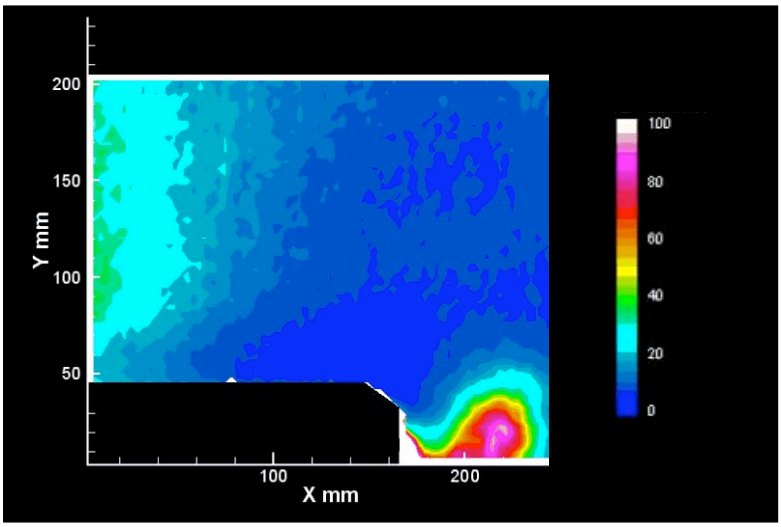

Figure 28

% Avg. Turbulence

Yaw = 20 deg

Bow and Side CVG

Rear View

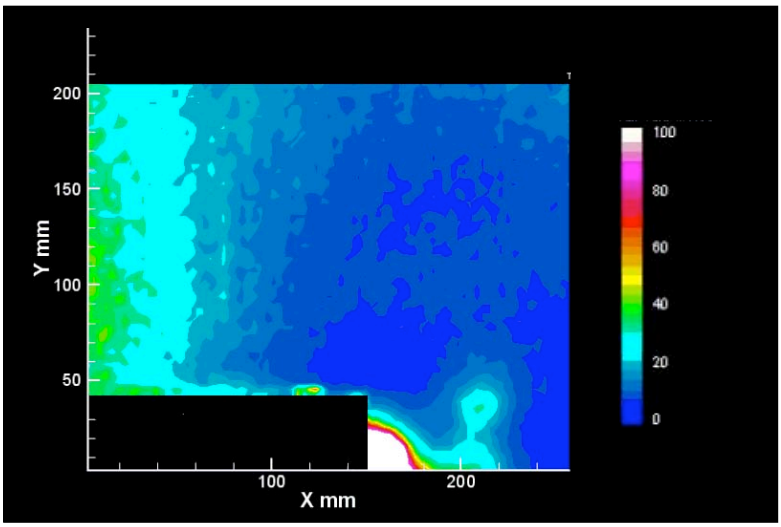

Figure 29

% Avg. Turbulence

Yaw = 20 deg

Bow and Side Flap

Rear View

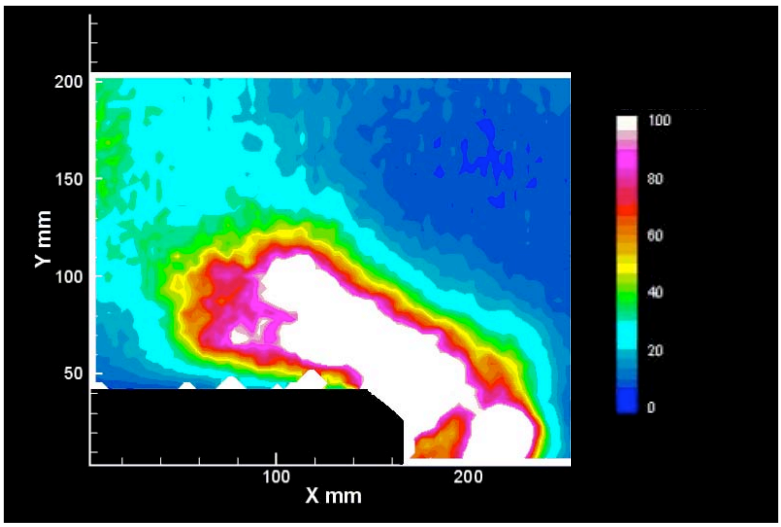

Figure 30

% Avg. Turbulence

Yaw = 20 deg

Side CVG only

Rear View

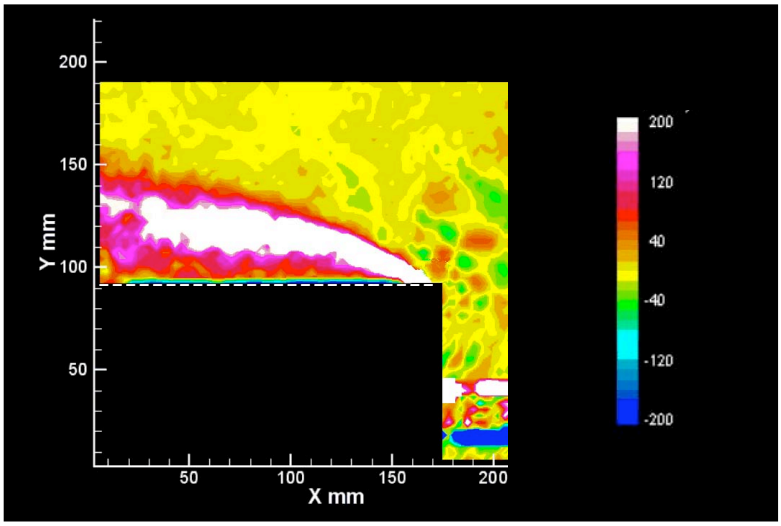

Figure 31

% Vorticity

Centerline

Yaw = 0 deg

Baseline Bow

Side View

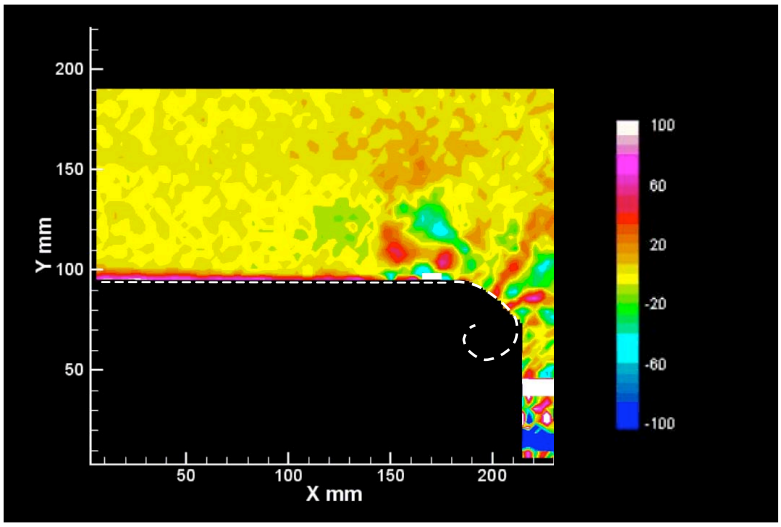

Figure 32

% Vorticity

Centerline

Yaw = 0 deg

Bow CVG

Side View